Materials & Design 221 (2022) 110985

Contents lists available at ScienceDirect

Materials & Design

journal homepage: www.elsevier.com/locate/matdes

Synthesis and performance of experimental resin-based dental adhesives reinforced with functionalized graphene and hydroxyapatite fillers

Nicoleta Ilie [a,*], Norbert Erich Serfözö [a], Doina Prodan [b], Julia Diegelmann [a], Marioara Moldovan [b]

[a] Department of Conservative Dentistry and Periodontology, University Hospital, LMU Munich, Germany
[b] Babes-Bolyai University, Institute of Chemistry Raluca Ripan, Cluj-Napoca, Romania

HIGHLIGHTS

- Nano-powders of functionalized graphene and hydroxyapatite were synthesized.
- Novel, non-toxic dental adhesives were formulated.
- In-vitro performance under clinically relevant environmental conditions and aging enables clinical use.

GRAPHICAL ABSTRACT

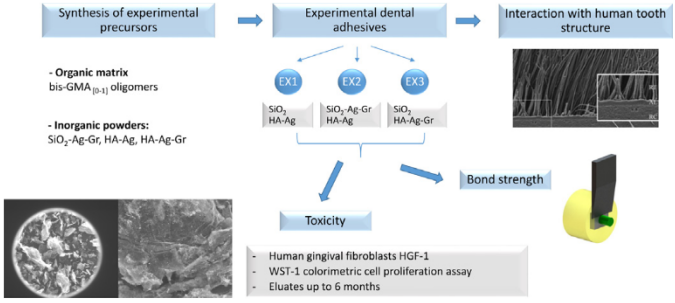

ARTICLE INFO

Article history:
Received 11 March 2022
Revised 22 July 2022
Accepted 22 July 2022
Available online 25 July 2022

Keywords:
Dentin adhesive
Graphene
Hydroxyapatite
Bond strength
Cytotoxicity
Fractography

ABSTRACT

Functionalized graphene and hydroxyapatite fillers are proposed as reinforcing particles in light-cured adhesives for dental applications. Silica-silver-graphene (SiO_2-Ag-Gr), silver-doped hydroxyapatite (HA-Ag), graphene and silver doped hydroxyapatite (HA-Ag-Gr), and regular silica (SiO_2) as inorganic powders, together with bis-GMA (2,2-bis[4-(2-hydroxy-3-methacryloxypropoxy) oligomers, as main components of the organic matrix, were synthesized. Light field transmission electron microscopy and electron diffraction proved the successful synthesis of the powders. The experimental adhesives showed a positive influence on local biocompatibility up to 6 months in an in-vitro simulation of clinically relevant environmental conditions and aging. Bonding to human dentin reveal a particular fracture pattern with preferential adhesion to the restorative material in contrast to the gold standard adhesive used as reference, which adheres preferentially to the tooth structure. Bond strength was slightly lower, initial bond reliability slightly improved, and the morphology of interaction with tooth structure similar to the reference. Functionalized graphene and hydroxyapatite fillers in dental adhesives have demonstrated their potential for use in dental applications.

1. Introduction

Dental caries is a major public health challenge worldwide, which places an enormous burden on the healthcare system [1]. To esthetically replace lost tooth tissue and carious defects, the use of adhesive, tooth-colored restorations [2,3] is the most common treatment, with resin-based composites (RBCs) being the

* Corresponding author: Department of Conservative Dentistry and Periodontology, University Hospital, LMU Munich Goethestr. 70, D-80336 Munich, Germany.
E-mail address: nilie@dent.med.uni-muenchen.de (N. Ilie).

https://doi.org/10.1016/j.matdes.2022.110985
0264-1275/

most popular restorative materials [4]. In contrast to their popularity, the decades-long debate about the superiority of RBCs over amalgam is still ongoing today. A recently published Cochrane study provides RBC restorations low-certainty evidence for both, a higher failure rate and a higher risk of developing secondary caries, compared to amalgam restorations [4]. The result is encouraging as mercury, the main component of dental amalgam, is considered an environmental pollutant and consistent efforts are being made to reduce the anthropogenic release of mercury into the environment from dental restorations, as required by the Minamata Convention [5].

In the complex interplay of factors that lead to failure of RBC restorations, comprising material properties, mechanical stress, biodegradation, secondary caries, and patient characteristics [6], dentin adhesives are attributed a strong influence [7]. The development of recurrent caries indicates that the seal at the interface between tooth structure and RBCs is insufficient to withstand the physical, chemical and mechanical stresses in the oral environment or the shrinkage forces encountered during polymerization [8]. As a consequence of these clinical observations, modern research is constantly striving to improve dental adhesives [7], while also taking into account achievements from other biomedical research or engineering areas [9]. This includes the incorporation of new types of reinforcement particles, which, in addition to the biocompatibility and caries-protective effects can also improve the mechanical properties and the bond to the tooth substance [7,10].

Recently, graphene has attracted the attention of biomedical research. First described in 2004 by Geim and co-workers [11], graphene is a planar nanosheet of sp^2-hybridized-single-atom-layer structure where the carbon atoms are packed in a two-dimensional honeycomb lattice [12,13]. It is a versatile material with a low production cost, great electrical (2.5×10^5 cm^2 V^{-1} s^{-1}) [14] and thermal conductivity (exceeding 3,000 W mK^{-1}) [15], a high elastic modulus (1 TPa), a high intrinsic strength (130 GPa) [16], and a large surface area. Graphene and its derivatives have already been successfully mixed into experimental dental materials [17]. Probably the greatest advantage of using graphene and its derivatives, such as graphene oxide (GO) and reduced graphene oxide (rGO), in dental materials, is the option of biological and chemical functionalization, in addition to the improvement in mechanical properties [18,19]. In this context, functionalization of GO with zirconium oxide (GO-ZrO_2) added as fillers in RBCs successfully improved the mechanical properties [20]. Graphene nanofibers used as fillers in polymethylmethacrylate (PMMA)-based CAD/CAM composites were shown to overcome the effects of age-related surface degradation on antimicrobial potential [21]. Small amounts (1 wt%) of GO and bioactive glass filler added to dental adhesives helped improve bond strength to tooth structure [22]. Similar results were also observed when 0.5 wt% and 2 wt% hydroxyapatite (HA)-coated GO fillers were incorporated into methacrylate-based adhesives, regardless of the aging process [23], as well as for 1 wt% GO, incorporated into an epoxy resin [24].

There is a whole range of materials that have been successfully incorporated into experimental dental adhesives as fillers. These includes nanoparticles of HA which, like the main tooth constituent, apatite crystals, have a remineralizing effect on tooth enamel [25] and the ability to improve bond strength to tooth structure [26,27] by reducing hybrid layer degradation [27]. Silica nanoparticles (SiO_2) help improve the mechanical properties of adhesives [7] and can be easily coupled by GO [28]. Such GO-SiO_2 nanoparticles incorporated into dental adhesives have been shown to maintain bond strength at levels as low as 1 wt% while increasing compressive strength compared to other commercially available adhesives [29]. The broad antimicrobial spectrum of silver nanoparticles, particularly in bacteria [30], has also been exploited [31] as they can cause rupture of the bacterial cell membrane, increase permeability and leading to cell death [30].

Building on the potential benefits and capabilities of the fillers described, we sought to synthesize a series of functionalized graphene and hydroxyapatite fillers for dental adhesives to improve biocompatibility and bonding to dentin. We hypothesize that the experimental adhesives will behave similarly to the gold standard adhesive in terms of: a) bond strength and interaction with dentin; b) behavior during aging; c) cellular toxicity up to 6 months.

2. Materials and methods

Three experimental two-steps *etch&rinse* adhesives were manufactured (Table 1) by photochemical initiation of polymerization. The adhesives were obtained by dispersing in a mixture of monomers based on experimental bis-GMA (2,2-bis[4-(2-hydroxy-3-methacryloxypropoxy) of inorganic filler particles based on: 1) silica-silver-graphene (SiO_2-Ag-Gr); 2) silver doped hydroxyapatite (HA-Ag); 3) hydroxyapatite doped with graphene and silver HA-Ag-Gr (HA-Ag-Gr); and 4) regular silica (SiO_2). The amount of inorganic filler in all experimental adhesives was 7% by weight. The experimental based monomer (93% 2,2-bis [p-(2-hydroxy- 3-methacryloyloxypropoxy)-phenyl]-propane monomer and 7% dimer) was synthesized by the reaction of the epoxy resin D.E.R.336 (Dow Chemical Company, Midland, Michigan, US) with the methacrylic acid [32]. The other components: triethylene glycol dimethacrylate (TEGDMA), hydroxyethyldimethylacrylate (HEMA), camphorquinone (CQ), dimethylaminoethyl-methacrylate (DMAEM) and additives (Merck, Darmstadt, Germany) were purchased (Sigma Aldrich Chemical Co., Taufkirchen, Germany). Both the experimental powder and the base monomer were synthesized in the "Polymeric Composites" laboratory of the Babes-Bolyai university, Institute for research in chemistry Raluca Ripan (ICCRR, Cluj-Napoca, Romania).

The bond strength and the morphology of the resin-dentin interface of the experimental adhesives to human dentine were evaluated in an initial immersion state (24 h) and after aging (6 months) according to methods unanimously accepted in dental research. The cellular toxicity at different time intervals up to 6 months was assessed on human gingival fibroblasts. The current gold standard adhesive was used as reference in all tests (Clearfill SE BOND 2, Kuraray Co.Ltd., Kurashiki, Japan, abbreviation CSE). A low shrinking bulk-fill RBC (Admira Fusion X-tra, Voco GmbH, Cuxhaven, Germany, abbreviation AF) was used as a restorative material.

2.1. Synthesis of the experimental precursors

2.1.1. Synthesis of bis-GMA

The organic matrix of the experimental adhesives consists of a mixture of monomers, in which the experimental bis-GMA is used as the base monomer and TEGDMA and HEMA are used as dilution monomers. The same proportions of monomers were used in each matrix of each experimental adhesive. Polyacrylic acid was added to create an acidic pH. The organic matrix consists of a monomer mixture of 97% by weight while the additives (polymerization initiator and accelerator, polymerization inhibitor, photosensitizer, antioxidant, UV stabilizer) were 3% by weight. The photoinitiator system consisting of the photosensitizer CQ (0.5 wt% relative to the liquid mixture) and the polymerization accelerator DMAEM (diethylaminomethyl methacrylate; 1 wt%) was incorporated into the dilution monomer mixture to which bis-GMA was then added.

Table 1
Chemical composition of the materials used indicated in mass %.

Code	Organic matrix	PAA	Ethanol	Inorganic filler	Lot №.
EX 1	bis-GMA oligomers, TEGDMA, HEMA	10	–	2 % SiO_2 5 % HA-Ag	–
EX 2	bis-GMA oligomers, TEGDMA, HEMA	10	5	0.2% SiO_2-Ag-Gr 6.8 % HA-Ag	–
EX 3	bis-GMA oligomers, TEGDMA, HEMA	10	5	2% SiO_2 5% HA-Ag-Gr	–
CSE	MDP, HEMA, DM	n.s.	n.s.	n.s	CF 0039
AF	ormocer	–	–	84.0% Ba-Al-Si-glass, SiO_2	1,537,600

Abbreviations: bis-GMA oligomers = (2,2-bis[4-(2-hydroxy-3-methacryloxypropoxy) phenyl]-propane); TEGDMA = triethylene glycol dimethacrylate; HEMA = 2-hydroxyethylmethacrylate, MDP = 10-methacryloyloxydecyl dihydrogen phosphate; DM = dimethacrylate; ormocer = organically modified ceramic; PAA = poly(acrylic acid), n. s. = not specified.

The bis-GMA $_{[0-1]}$ oligomers were synthesized by the reaction of the epoxy resin D.E.R.336 (Dow Chemical Company, Midland, Michigan, US) with the methacrylic acid, in the presence of a basic catalyst, at temperature of 60 °C and in the absence of solvents. The reaction was carried out in a glass reactor fitted with a flanged cap and four necks for a mechanical stirrer, a condenser and a thermometer. The inhibitor BHT (2,6-di-*tert*-butyl-4-methylphenol; Merck) and the catalyst TFF (triphenylphosphine, Merck) were dissolved into the methacrylic acid. The reaction mixture was maintained at a temperature of 60 °C and continuously stirred for 24 h, followed by analytical conversion of methacrylic acid. The reaction was considered complete when the concentration of methacrylic acid in the reaction mixture was below 0.5%. The conversion of methacrylic acid was determined by titrating the acid in the reaction mixture with 0.1 N NaOH using acetone as solvent and bromothimole blue as indicator.

The synthesized inorganic fillers described below were added to the monomer mixture in a darkroom to avoid premature polymerization. A T18 disperser (IKA®-Werke GmbH & Co. KG, Staufen, Germany) was used to mix the monomers with the inorganic powders at 700 rpm for 15 min.

2.1.2. Synthesis of hydroxyapatite (HA)

HA was obtained by wet chemical methods (precipitation technique) [33], whereby the raw materials, the reaction conditions and the heat treatment were varied.

The synthesis starts with calcium hydroxide [$Ca(OH)_2$] 0.5 M (the result of the hydrolysis of 3% by weight calcium oxide (CaO) and 97% by weight distilled water) and orthophosphoric acid (H_3PO_4) 0.3 M in stoichiometric proportions, as raw materials (Equation (1)). The reaction temperature was adjusted to 80 °C for 3 h, the pH being maintained at 7.5 by dropwise addition of a 3% ammonia solution. The reaction product was a translucent gel, which was then left at room temperature (23 °C) for 70 h to mature.

$$6H_3PO_4 + 10Ca(OH)_2 = Ca_{10}(PO_4)_6(OH)_2 + 18H_2O \quad (1)$$

The maturation process is expected to induce pH changes through hydrolysis of the phosphate precursor. The hydrolysis products then form a complex with calcium ions in the solution. After maturation, the hydrolyzed phosphorus soil probably interacted with the calcium soil and formed derivatives containing the Ca-O-P base group.

2.1.3. Synthesis of hydroxyapatite-silver (HA-Ag) particles:

The silver nitrate ($AgNO_3$) was added to the obtained HA gel described above. The $AgNO_3$ solution was obtained by dissolving 0.02% $AgNO_3$ in 99.98% H_2O. Next, NH_3 concentrate was added dropwise under continuous stirring with a magnetic stirrer to obtain a soluble complex. The initial pH of the solution, which is the precursor to obtaining Ag nanoparticles, was 11. During the reaction, a glucose reducing mixture of 0.01 M and hydrazine hydrate of 0.01 M was added dropwise into the solution. A pH of 7.4 was reached by dropwise addition of a 1 M citric acid solution. The obtained Ag nanoparticles gel was then poured over the HA gel at 80–90 °C and continuously stirred for another hour. The following day, the resulting mixture was filtered under vacuum conditions through a Buchner funnel, consisting of a blue and a double filter strip. The filtrate was washed 2–3 times with distilled water, then transferred to a large porcelain capsule and placed in the drying oven at 80 °C for four hours. The powder obtained was sieved and placed in a drier using a plastic vial to avoid particle agglomeration. Subsequent drying, during which the product was heated, leads to the removal of the solvent, probably accompanied by dehydration and polymerization/condensation of these groups, and the formation of many Ca—O—P bonds in the dry gel. The slow evaporation provides not only the conditions of intimate interaction but also thermal energy for the process.

2.1.4. Synthesis of graphene–silver particles (Gr-Ag)

GO was prepared by oxidation of graphite (99.9%, Alfa Aesar) using the Hummer method [34]. One g graphite and 0.5 g of sodium nitrate were slowly added to 23 mL concentrated H_2SO_4 and stirred for 1 h. Then 3 g of $KMnO_4$ was carefully added, keeping the temperature below 15 °C to avoid overheating. The mixture was stirred for 3 h. Forty-six mL of deionized water was added very slowly to the mixture. After 30 min, the reaction mixture was diluted with 140 mL of deionized water. The reaction was quenched by the addition of 10 mL of 10% H_2O_2. The oxidized product was washed seven times with 5% HCl to remove metal ions, followed by eight washes with deionized water to remove the remaining acid. The product thus obtained was dried at 50 °C for 24 h to obtain GO sheets. 0.04 g GO were then dispersed in 100 mL distilled water, followed by ultrasound (ELMA Hans Schmidbauer GmbH & CO, Singen, Germany) for 30 min at 60 °C. The solution of the Ag nanoparticles (described in 2.1.3) was dropped over this solution and a precipitate was formed. It was then centrifuged, washed with 40% alcohol, and dried at 45 °C.

2.1.5. Synthesis of the silica particles (SiO_2) / synthesis of the silica-silver-graphene particles (SiO_2-Ag-Gr)

To obtain SiO_2 particles, the sol–gel reaction was started from 30.9% to 68.5% colloidal silica mixed with distilled water in which 0.6% HNO_3 was dissolved. Mixing was done with a mechanical stirrer at room temperature for 1–2 h. The mixture was then left until the next day. The previously synthesized, weighed Gr-Ag nanopowders were mixed with 1:2 distilled water. The suspension thus obtained was introduced into the ultrasonic bath (ELMA Hans Schmidbauer GmbH & COy) for 2 h at maximum frequency. After ultrasound, the suspension was added to the SiO_2 gel and stirred at room temperature for 8 h. This was followed by filtering and

drying the paste in a vacuum oven at 120 °C for 4 h. The powder obtained was sieved and stored at room temperature.

2.1.6. Synthesis of the hydroxyapatite-silver-graphene particles (HA-Ag-Gr)

For the HA-Ag-Gr synthesis, the HA and Gr-Ag powders obtained by the methods described above were used. In two separate vessels, equal proportions of HA / distilled water and Gr-Ag / distilled water were added and were ultra-sonicated for one hour at maximum frequency. After the sonication, the suspensions were mixed and sonication continued for a further two hours. This was followed by filtration and drying, similar to the steps described in 2.1.5., after which the powder obtained was sieved and stored at room temperature until use.

All fillers were silanised using γ-methacriloyloxypropyl-tryme thoxysilane (A-174, Sigma-Aldrich Inc., St. Louis, MO, USA) hydrolyzed in acidified alcoholic solution at pH 3.5–4.

2.2. Synthesis of the experimental adhesives

The chemical composition of the three experimental adhesives is listed in Table 1. The synthesized inorganic fillers described above were added to the monomer mixture in a darkroom to avoid premature polymerization. A T18 disperser (IKA®-Werke GmbH & Co. KG, Staufen, Germany) was used to mix the monomers with the inorganic powders at 700 rpm for 15 min.

2.3. Shear bond strength (SBS) test

Forty freshly extracted human third molars (preserved in a 0.4 % sodium azide solution at a temperature of 4 °C) were selected and cleaned from adherent tissue and debris. Teeth were cut horizontally 2 mm under the central groove in a vestibular lingual direction using a water-cooled low speed diamond saw (Isomet, Buehler, Lake Bluff, IL, USA). Another cut was performed perpendicular to the previous one, resulting in four segments. The 160 tooth segments were then randomly divided into 4 groups (n = 40). Each tooth segment was embedded in a methacrylate resin (Technovit 4004, Kulzer, Wasserburg, Germany) using a steel cylinder (h = 19 mm, Φ = 19 mm).

To produce a standardized dentin smear layer, the surface of each segment was ground using 600 grit silicon carbide abrasive paper (Hermes, EXAKT Advanced Technologies GmBH, Norderstedt, Germany) by means of a grinding and polishing machine (Leco Corp. SS-200, MI, USA) [35,36]. Dentin surfaces were subsequently etched with a 35% phosphoric acid (K-Etchant, Kuraray Co.Ltd., Kurashiki, Japan) for 15 s, followed by water rinsing and air drying. Next, the experimental adhesive was applied on dentin surfaces with a disposable microbrush for 10 s and then air dried for 5 s. The adhesive surface was light cured for 20 s using a LED (Light Emitted Diode) light curing unit (LCU) (Bluephase Style, Ivoclar-Vivadent, Shaan, Lichtenstein). The irradiance, radiant exposure, and spectral distribution of the LCU were measured using a spectrophotometer (MARC-RC (Managing Accurate Resin Curing), Bluelight Analytics Inc., Halifax, Canada). Subsequently, a silicon mold (h = 4 mm, Φ = 3 mm) was adapted on the specimens and filled in one increment with a low-shrink bulk-fill RBC (AF), which was light-cured for 20 s with the LCU described above. The bonded tooth-samples were stored in distilled water in a dark environment for 24 h at 37 °C. Half of the samples from each group were additionally subjected to thermal aging (abbreviated TC, 10,000 cycles between 5 °C and 55 °C, dwell time 30 s, transfer time 5 s, Willytec, Dental Research Division, Munich, Germany). All specimens were loaded onto a universal testing machine (Z2.5, Zwick Roell, Ulm, Germany). A load was applied at the adhesive interface at a cross-head speed of 0.5 mm/min, until fracture. The shear bond strength (MPa) was calculated by dividing the load of fracture (N) to the surface bonded area (mm^2).

2.4. Fractography

The fractured segments were examined using stereomicroscopy (Stemi 508, Carl Zeiss AG, Oberkochen, Germany). All samples failed adhesively, making all data valid for the SBS test. A modified adhesive remnant index (mARI) was used to quantify the residual adhesive on the dentin surface after fracture (Table 2). The mARI index was quantified using the Axio Vision computer software (Carl Zeiss AG).

2.5. Scanning electron microscopy (SEM) evaluation

Four randomly selected dentin slices were assigned to each adhesive group. The same methods as described above were used to create the smear layer, etch the dentin and apply the adhesive. The RBC was applied on the whole exposed dentin surface. Cross-sections of each specimen, exposing the dentin–adhesive–RBC interface were embedded in a methacrylate resin using a steel cylinder. The exposed dentin-adhesive-RBC interface of each specimen was wet finished with a series of silicon carbide abrasive papers (1200 grit, 1500 grit, 2000 grit, 2400 grit) and then polished with diamond sprayed (6 μm, 3 μm, 1 μm; DP-Spray, Struers GmbH, Puch, Austria) and textile polishing cloths (DP-Pan 200 mm, Struers GmbH). All samples were cleaned ultrasonically (RK 31, Badelin Electronic, Berlin, Germany) for 5 min after each polishing step. Samples were then demineralized with a 6 N hydrochloric acid solution (Sigma-Aldrich Co., St. Louis, Missouri, USA) followed by a deproteinization in a 12% sodium hydroxide solution (Sigma-Aldrich Co.). The samples were then rinsed with distilled water, air dried, followed by dehydration in ascending ethanol solution (25% for 20 min, 50% for 20 min, 75% for 20 min, 95% for 30 min, and 100% for 1 h) prior to scanning electron microscopy examination. All dehydrated specimens were mounted on aluminum stubs and sputtered with gold. Micrographs were taken using a scanning electron microscope (Zeiss Supra 55 V P, Carl Zeiss AG, Oberkochen, Germany) operating at 10 kV in three randomly selected sections at a magnification rate of 500x to evaluate the thickness of the adhesive layer and the penetration number of the resin tags in the dentinal tubules. Adhesive layer thickness (μm) was measured at five randomly selected locations on the resulting images. The dentin-adhesive interface was then divided into equal sections of 50 μm and the resin tags were counted within each section. The resin tag penetration number (RTPN) was expressed as the number of resin tags per 50 μm. Micrographs analysis was performed using Adobe Photoshop computer software (Version 7.0, Adobe Inc., San Jose California, USA).

2.6. Transmission electron microscopy (TEM, HRTEM) images of synthesized inorganic fillers

The morphological characteristics of the synthesized powders were analyzed by transmission electron microscopy (Hitachi 120 kV TEM model H-7650, Hitachi High-Tech Corporation,

Table 2
Modified adhesive remnant index (mARI) with the percentage of residual adhesive on the dentin surface after fracture.

mARI	residual adhesive
0	0% to 25%
1	25% to 50%
2	50% to 75%
3	75% to 100%

Hitachinaka, Ibaraki, Japan) and by high resolution transmission electron microscopy (Tecnai F30 G2, FEI Company, Hillsboro, OR, USA) at a linear resolution of 1 Å and a point resolution of 1.4 Å. To do this, small amounts of the powder were immersed in absolute ethyl alcohol, with the suspension being homogenized by ultrasound. Fine particles were collected from the homogenized suspension using a copper grid covered with a very thin layer of carbon (with holes). The samples thus obtained were used to characterize the morphology of the synthesized fillers.

2.7. Cell culture

Human gingival fibroblasts HGF-1 (ATCC® CRL-2014™) were cultured in Dulbecco's Modified Eagle's high glucose Medium (Sigma-Aldrich Co.) supplemented with 10% fetal bovine serum (FBS) and 1% penicillin/streptomycin (PenStrepFa, Sigma-Aldrich Co.) using sterile cell culture dishes (CellStar®, Greiner Bio-One International GmbH, Kremsmünster, Austria) with the nominal size of 100/20 mm. Cells were incubated in a humidified CO_2 incubator (Heracell 150i, Thermo Scientific, Waltham, MA, USA) at a temperature of 37 °C, 5% CO_2 and a 95% air atmosphere. The medium was changed 3 times weekly, and the cells were monitored using an inverted phase-contrast microscope (Axiovert 40C, Carl Zeiss AG). Upon reaching an 80% confluence, cells were rinsed with Dulbecco's phosphate-buffered saline (Sigma-Aldrich Co.) and detached with a trypsin-EDTA solution (0.25% trypsin, 0.53 % mM EDTA). Cell counting was performed using a mix of 10 μL cell suspension and 10 μL trypan blue solution (Sigma-Aldrich Co.), added to a counting chamber (Neubauer Improved Haemocytometer, Paul Marienfeld GmbH & Co. KG, Lauda-Königshofen, Germany). Cells were used between passage 7 and 13 for all assays.

2.8. Preparation of test specimen and eluates

Freshly extracted human third molars preserved and treated as described above were cut horizontally in 2-mm thick slices. The surfaces of 41 dentin slices were measured by means of stereomicroscopy using a microscope camera extension. Dentin slices were then sterilized and redistributed to each adhesive group. Bonding application on each dentin surface occurred under sterile conditions in a horizontal laminar airflow clean bench (Holten LaminAir, Thermo Scientific, Waltham, MA, USA). Bonded dentin slices were added to 3 mL of complete cell culture medium in 15 mL conical tubes (Falcon, Becton, Dickinson and Company, Franklin Lakes, NJ, USA) to fulfil the recommendation of ISO 10993–12, which stipulates a ratio of 117.8 mm^2 sample surface area/mL cell culture medium [37]. The samples were incubated at 37 °C and eluates from each adhesive group and control media without test specimen were prepared in triplicates and were collected after 24 h, 48 h, 72 h, 10 days as well as after 1, 3 and 6 months. Culture medium was collected and replaced with 3 mL of fresh culture medium. At each time point, the collected cell culture medium was frozen at −20 °C prior to testing.

2.9. Cytoxicity assay

To examine the influence of the various adhesive's eluates on cell viability, a WST-1 (4-[3-(4-Iodophenyl)-2-(4-nitro-phenyl)–2 H-5-tetrazolio]-1,3-benzene sulfonate) colorimetric cell proliferation assay (Sigma-Aldrich Co.) was performed. The tetrazolium salts of this assay are cleaved to formazan by the cellular mitochondrial dehydrogenases. There is a direct correlation between the number of metabolically active cells and the amount of formazan dye produced. The absorbance of the dye was measured spectrophotometrically [38].

Cells were seeded into 96 well cell culture plates (Greiner Bio-One International GmbH, Kremsmünster, Austria) in 100 μL of cell culture medium at a density of 10,000 cells per well. Twenty-four hours after seeding, the cell culture medium in each well was replaced with eluates and control media collected at the respective time period and the cells were incubated for 24 h in the humidified CO_2 incubator. Ten μL of cell proliferation reagent WST-1 were added to each well, and the plates were incubated for two hours in the CO_2 incubator at 37 °C before reading the optical density (OD). Wells without cells served as blank control. OD was measured according to the manufacturer's standard protocol at 440 nm and a reference absorbance at 600 nm [38], using a scanning multiwell spectrophotometer (Varioskan LUX Multimode Microplate Reader, Thermo Scientific) and SKanIT RE for Varioskan (Ver.2.2, Thermo Scientific) computer software.

Absorbance at 600 nm was subtracted from that obtained at 440 nm to account for background variation of the plate. The viability of the cells was calculated as a percentage of cell viability compared to the negative control (untreated cells) using the following equation:

$$V = \frac{(A440 - A600)_{treated}}{(A440 - A600)_{control}} \quad (2)$$

with V = cell viability and A = absorbance.

A cell viability of 100% was attributed to the HGFs grown in the control cell culture medium collected at the respective time point. Samples of each material at a given time point were tested in triplicates. Results interpretation was made according to ISO 10993–5 [39].

2.10. Statistical analysis

Normal distribution was verified by a Kolmogorov–Smirnov test. Equality of variances was determined by a Levene's test. For the SBS and the cell toxicity data, a two-way ANOVA test, Student's t-Test, and Games Howell post–hoc test were employed. The mARI score was evaluated with the Fisher-Freeman-Halton Exact Test (alternative for the Chi^2 Test) followed by Z-Test for column proportion comparison with adjusted p values (Bonferroni method). The adhesive layer thickness and the RTPN were evaluated by means of one-way ANOVA, Welch test (for variance heterogeneity), followed by Tukey's HSD post-hoc test for equal distributed variances and Games Howell post–hoc test for unequal distributed variances. The results from each test were considered significant for $p \leq 0.05$ (95% confidence level). In addition, a partial eta-squared statistic indicates the practical relevance of each term, based on the ratio of the variation attributed to the effect. Data were analyzed using the SPSS computer software (IBM SPSS Statistics, Version 27, International Business Machines Corporation, NY, USA).

The reliability of the bond strength to dentin was quantified by Weibull analysis. The Weibull model describes the probability of failure F at uniform stress σ using the following formula:

$$F(\sigma_c) = 1 - e^{-(\sigma_c - \sigma_0)^m} \quad (3)$$

Where m is the Weibull modulus, σ_c is the measured strength, σ_0 is the characteristic strength at probability of failure $F(\sigma_f) = 0.63$.

The double logarithm of this expression: $\ln\ln\frac{1}{1-F(\sigma_c)} = m\ln(\sigma_c) - m\ln(\sigma_0)$ results in a straight line, whereas the upward gradient of this line is represented by m. Subsequently, the intersection with the x-axes results in the logarithm of the characteristic strength σ_0.

3. Results

3.1. LCU characteristics

The used polymerization device was a violet-blue LED-LCU evidencing two distinct emission peaks, one at 410 nm in the violet wavelength range and one at 454.8 nm in the blue wavelength range (see Fig. 1). The irradiance (n = 5), measured by placing the LCU tip in direct contact with the sensor, was (1,386 ± 29.1) mW/cm^2. The used photoinitiator in the experimental adhesives as well as in the gold standard reference adhesive was camphorquinone (CQ), a di-2,3-diketo-1,7,7-trimethylnorcamphane with an absorption peak at 470 nm. The emission spectrum of the LCU in the blue wavelength range therefore ideally matches the absorption spectrum of the initiator CQ.

3.2. Shear bond strength (SBS) test

The SBS and Weibull statistics for each adhesive group and aging condition are presented in Table 3 and Fig. 2. A two-way ANOVA analysis identified statistically significant effects of the parameters "adhesive" ($p = 0.009$, $\eta_P^2 = 0.456$), "TC" ($p < 0.001$, $\eta_P^2 = 0.044$), and the interaction of both ($p < 0.001$, $\eta_P^2 = 0.109$). The highest SBS was achieved in the reference group, CSE, in both 24 h (10.0 ± 3.2) MPa and TC groups (12.2 ± 5.2) MPa. No statistically significant differences were observed among EX1, EX2, and EX3 in both 24 h and TC groups. A statistically significant decrease in SBS after TC compared to the 24 h storage (multiple independent Student's *t*-test) was observed in all experimental groups while the results were maintained in the control group CSE ($p = 0.16$). EX1 achieved the highest Weibull modulus at 24 h. Aging resulted in a decrease in Weibull's modulus in all experimental adhesives, but not in the reference CSE, where it remained constant.

The fractographic analysis shows that all fractures occurred adhesively. The Fisher-Freeman-Halton exact test indicates a significant dependency ($p < 0.001$) between the adhesive used and the mARI score in both 24 h and TC groups. Table 4 shows the distribution count and percentage of each adhesive group in correlation with the mARI score.

The adhesive layer thickness and the RTPN values are listed in Table 5. EX1 and CSE showed statistically similar and the highest values for the adhesive layer thickness ($p = 0.497$) and RTPN ($p = 0.840$). SEM images in Fig. 3 evidenced the formation of dense resin tags and a uniform adhesive layer for both adhesives. In contrast, longer resin tags are observed for EX3, while they were fewer for EX2.

The morphology of the synthesized particles using light-field transmission electron microscopy and the associated electron diffraction imaging (SAED) is shown in Fig. 4a and 4b.

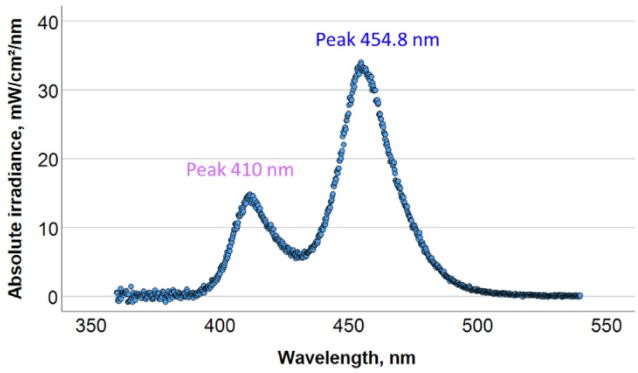

Fig. 1. LCU: Emission spectrum measured by placing the LCU tip in direct contact with the sensor.

With regard to cellular toxicity, significant effects of the parameters "adhesive" ($p < 0.001$, $\eta_P^2 = 0.129$), "elution time" ($p < 0.001$, $\eta_P^2 = 0.320$), and the interaction between "adhesive and time" ($p < 0.001$, $\eta_P^2 = 0.362$) were detected. Fig. 5 shows the percentage of HGF-1 cell viability exposed to eluates from different adhesive groups at different elution times, including the negative control (NC). Eluates from CSE had the significant lowest cell viability (53%) at 24 h of elution. After 48 h elution, the adhesive group EX3 had statistically significant lower cell viability values (74%) compared to the other groups EX1 (105%), EX2 (129%), CSE (108%) but not to the NC. After 72 h elution, no significant cell toxicity was detected in any of the adhesive groups. Higher toxicity was again observed in eluates from day 10, in which cell viability was significantly lower than in the NC for all adhesive groups EX1 (72%), EX2 (75%), EX3 (50%) and CSE (74%). After 1, 3 and 6 months no statistically significant differences between the adhesive groups could be observed.

4. Discussion

The study describes the successful syntheses of functionalized graphene and hydroxyapatite nano-powders and their implementation into experimental dental adhesives. The selection of the synthesized powders - SiO_2-Ag-Gr, HA-Ag, HA-Ag-Gr and SiO_2 - was motivated by a number of positive aspects described in the literature, mainly related to enhanced bioactivity [40–42] and remineralization effects [43–45] and supported by preliminary evidence that the durability of the adhesive-dentine interfaces can be improved by modified bonding agents [10].

One of the mechanisms of how GO works from a microbiological point of view is related to its particular geometry. The sharp edges and corners of GO layers can penetrate the cell membranes of bacteria, leading to leakage of the intracellular cytoplasm and cell death [40]. In the event GO sheets do not penetrate the bacterial cell membrane, their large specific surface area allows attachment to the cell surface, isolating them from the external environment and the nutrients necessary for survival, and reducing glucose consumption [41]. The antibacterial potential of GO can be even accelerated through a third mechanism that involves the inherent acidic impurities generated during the manufacturing process that can dissolve in the bacteria's environment [42]. The functionalization of GO with Ag performed in the present study additionally increases the antibacterial activity compared to the antibacterial activity of each component used separately, as GO and Ag act synergistically [42]. The functionalization was possible due to the presence of the oxygen functional groups (hydroxy, epoxy and carboxy) on the surface and on the edges of GO sheets. Positively charged Ag^+ ions can then bind to the surface of negatively charged GO sheets either through charge transfer, physical absorption, or electrostatic bonding [46].

In addition to the antibacterial effect described above, GO can also enhance the remineralization potential of the material in which it is contained. Even small amounts of GO added to the organic matrix of dentin adhesives can contribute to remineralization of the adhesive-dentin interface due to the hydrophilic nature of GO, which can attract calcium ions contributing to the formation of HA [44] and the formation of the hybrid layer [45]. On a similar note, remineralization of the adhesive-dentin interface can be achieved by adding silica nano-particles to the adhesive, as silica act as a nucleating mineral and promote the formation of calcium-phosphate precursors [47]. The presence of silica in the adhesive ensures that calcium is attracted to develop a stable bioactive calcium silicate compound that can bind to phosphorus [43]. Along with its role in the remineralization process, silica has a mechanically reinforcing effect on the adhesive, but do not

Table 3
Shear bond strength in MPa (mean ± standard deviation), and Weibull modulus with confidence interval in brackets. Superscripts indicate statistically significant differences within adhesives per storage (per column; Games Howell post-hoc test, $\alpha = 0.05$). Capital letters indicate statistically significant differences within one material due to aging (per row; independent student's *t*-test, $\alpha = 0.05$).

Adhesive	Shear bond strength (SBS)		Weibull modulus (m)	
	24 h	TC	24 h	TC
EX1	5.4 ± 1.9 [a] A	3.6 ± 2.0 [a] B	3.4 [2.8–4.0]	1.9 [1.7–2.0]
EX2	6.1 ± 2.4 [a] A	6.1 ± 2.4 [a] A	3.1 [2.7–3.7]	1.4 [1.0–1.9]
EX3	6.0 ± 2.0 [a] A	3.9 ± 3.0 [a] B	3.0 [2.8–3.3]	1.5 [1.2–1.8]
CSE	10.0 ± 3.2[b] A	12.2 ± 5.2[b] A	2.6 [2.5–2.8]	2.9 [2.3–3.5]

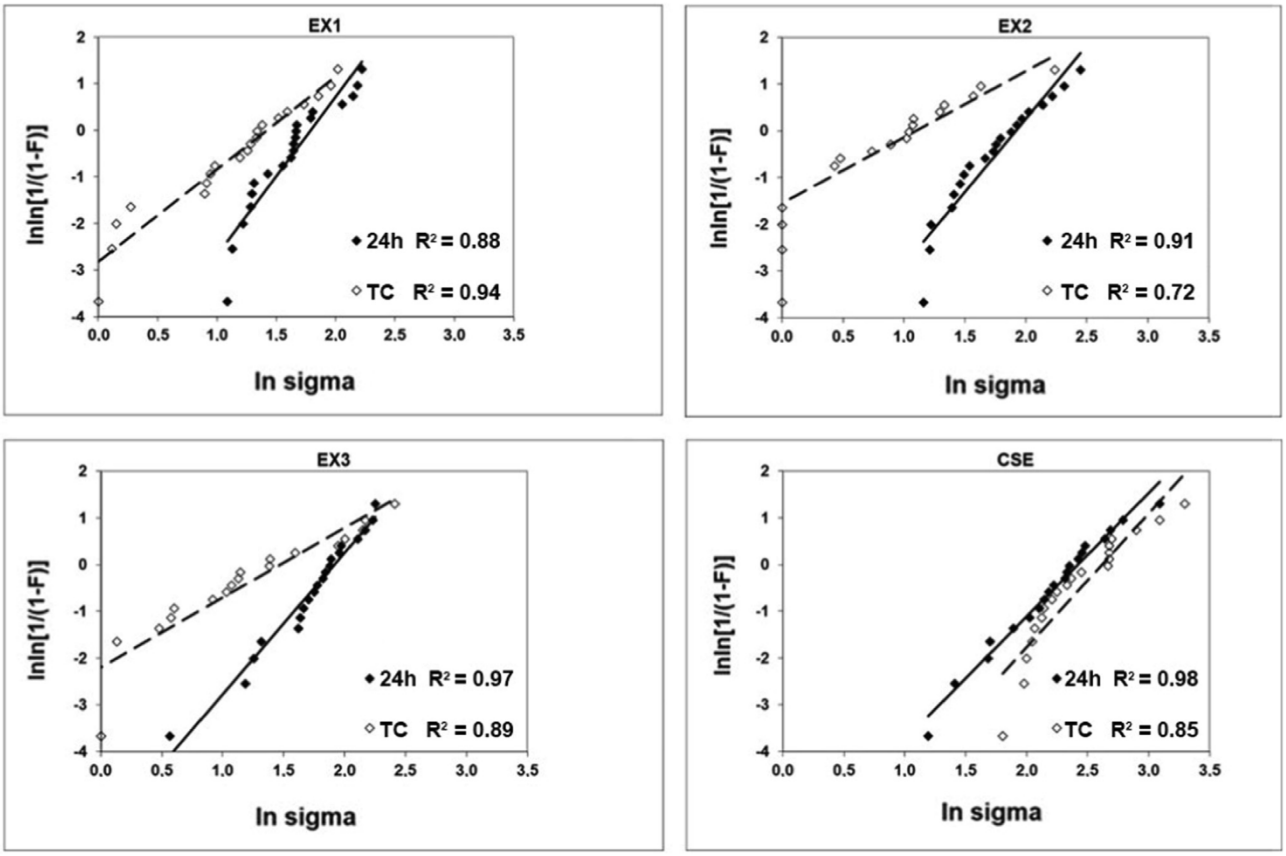

Fig. 2. Weibull distribution as a function of material and storage.

Table 4
Samples count and attributed percentage for each adhesive group in correlation with mARI score for both 24 h and aging groups (Fisher-Freeman-Halton exact test). Lowercase letters indicate statistically significant differences between the adhesive groups within one score value of the mARI Index (Z-Test with adjusted p values, Bonferroni method).

Adhesive (24 h)					Adhesive (TC)						
mARI	EX1	EX2	EX3	CSE	mARI	EX1	EX2	EX3	CSE		
0	Count	20_a	18_a	19_a	0_b	0	Count	20_a	19_a	19_a	1_b
	%	100	90	95	0		%	100	95	95	5
1	Count	0_a	1_a	1_a	3_a	1	Count	0_a	1_a	0_a	5_a
	%	0	5	5	15		%	0	5	0	25
2	Count	0_a	1_a	0_a	3_a	2	Count	0_a	0_a	1_a	3_a
	%	0	5	0	15		%	0	0	5	15
3	Count	0_a	0_a	0_a	14_b	3	Count	0_a	0_a	0_a	11_b
	%	0	0	0	70		%	0	0	0	55

affect the rheology and therefore the flowability of the adhesive, which allows penetration of the dentin tubules and the formation of stable resin tags after polymerization [10].

In addition to the synthesized powders, the bis-GMA that served as polymer matrix for the experimental adhesives was synthesized to produce materials with full control over each individual component. As the experimental adhesives are potential materials for use in a clinical situation, their performance was compared to the current gold standard, a mild self-etch adhesive, in terms of their toxicity, ability to bond and interact with the

Table 5
Adhesive layer thickness (μm) and the number of resin tags/50 μm (RTPN); Mean values ± standard deviation. Different superscript letters indicate statistically significant differences within the 4 materials. Games-Howell post-hoc test (α = 0.05) / Tukeýs HSD post-hoc test (α = 0.05).

Adhesive	Adhesive layer thickness	RTPN
EX1	10.0 ± 1.7 [a]	28.1 ± 8.1[c]
EX2	5.9 ± 3.3[b]	16.7 ± 8.0 [a]
EX3	7.8 ± 2.5[b]	19.7 ± 7.5 [ab]
CSE	8.1 ± 9.9 [ab]	24.4 ± 5.7 [bc]

tooth structure as well as the way they performed during aging. The slightly higher bond strength observed in the reference can be explained by the additional use of a primer before applying the adhesive, as part of a self-etch approach. Like the reference adhesive, the primer contains the functional monomer 10-methacryloyloxydecyl dihydrogen phosphate (10-MDP) which is able to chemically interact efficiently with the dentine HA due to a lower decalcification effect. The calcium salt formed as a result of this interaction is hardly soluble, which is reflected in a stable bond strength to dentin in time [48]. An interaction of 10-MDP with collagen [49] is also described, involving hydrophobic moieties of 10-MDP and the hydrophobic collagen surface, thereby enhancing adhesion to dentin and impeding long-term degradation. Also, the use of mild self-etch adhesives allows collagen to remain encapsulated and protected by HA and not to collapse. In contrast, the experimental adhesives involve a phosphoric acid etching step that exposes dentinal collagen, making it highly susceptible to hydrolytic and enzymatic degradation processes [50]. Also detrimental is the fact that dimethacrylate polymers can adsorb water, which can enter the polymer network either via capillarity, diffusion, or micro-cracks [51] making hydrolytic degradation one of the more difficult challenges of this category of materials [52]. As a result, polymers swell and soften, which can lead to a deterioration in their mechanical properties. The water sorption depends on the crosslink density of the polymer chain and the chemical structure of the monomer [53]. The degradation potential therefore lies in the nature of the materials, since there are a number of hydrolysable bonds such as esters and ethers, which can be cleaved by hydrolysis [54]. Although the bis-GMA monomer incorporated in the experimental adhesives is considered to be relatively hydrophobic, it contains both hydrophobic and hydrophilic components. While the core of the monomer, diphenylisopropane, provides hydrophilicity, the two hydroxyl groups induce hydrophilicity. Besides, the diluent monomer HEMA included in the experimental adhesives is characterized by high water sorption [55], while the poly(HEMA) formed after polymerization behaves like a hydrogel and absorbs water too. The repetitive temperature changes during the 10,000 thermal cycles between 5 °C and 55 °C used to age the bonded specimens in the present study, result in volume changes, causing water to enter the free volume, ultimately resulting in weaker bond strengths to dentin. This was evident in significantly reduced bond strength values in two of the experimental adhesives during aging. The incorporation of HA, GO and silica particles into the experimental adhesives aimed to improve mechanical properties and contribute to the remineralization of the previously acid-etched dentin, as earlier described, but this effect may have been overshadowed by water sorption and its detrimentally effects, since we used an accelerated aging procedure, while remineralization is a consistently slower process. Since the amount of filler was the same in all experimental adhesives, the high mechanical properties of GO contained in the fillers of EX2 and EX3 could not improve the bond strength compared to EX1 where GO is absent. However, in terms of bond reliability, well characterized by the Weibull model (high R^2 values, Table 1), the experimental adhesives behaved similarly at an earlier stage of aging and were superior to the gold standard reference. These initial benefits were then mitigated by aging, presumably due to the 10-MDP content in the primer of the reference adhesive chemically interacting with the HA of the tooth, according to the arguments exposed previously. This assumption is supported by the fractographic analysis and the mARI index, as a

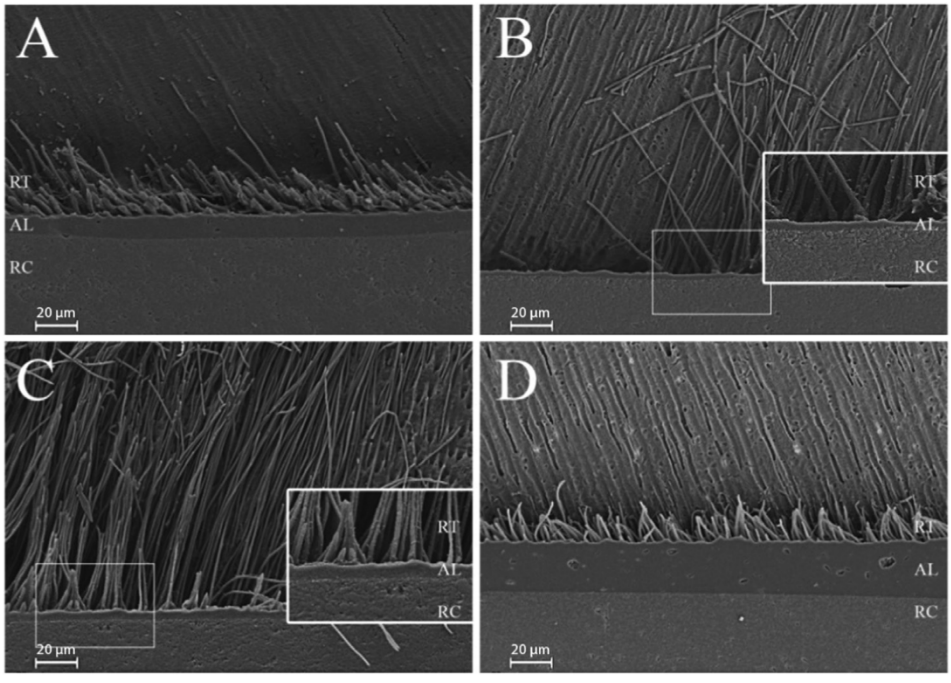

Fig. 3. SEM images of the different adhesive groups: (A) EX1, (B) EX2, (C) EX3, and (D) CSE. RT = resin tags, AL = adhesive layer, RC = resin composite. The images show differences in resin tag formation, number, and depth of penetration in the dentinal tubules of the different adhesive groups. Differences in the adhesive layer thickness can also be seen between the different adhesive groups.

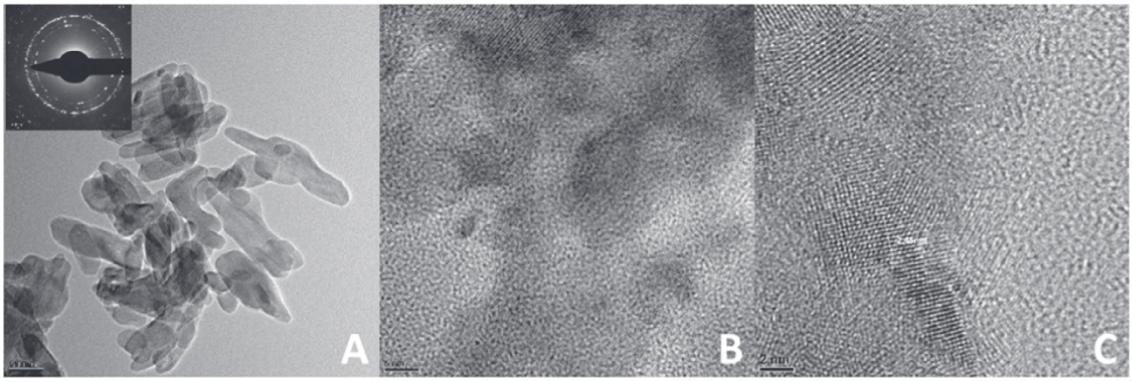

a) HA-Ag: A) Light field transmission electron microscopy imaging showing a set of hydroxyapatite and silver nanoparticles in form of rods; B) and C) associated electron diffraction imaging (SAED) with high resolution transmission imaging (HRTEM) evidencing a HA nano-crystalline area at two different resolutions. The very bright spots belong to large HA crystallites and the small spots correspond to very small nanocrystals. Diameter diffraction circles correspond to interplanetary distances specific to the families of crystalline planes (indexed in the image) of the compound $Ca_5(PO_4)_3OH$ with hexagonal crystal lattice.

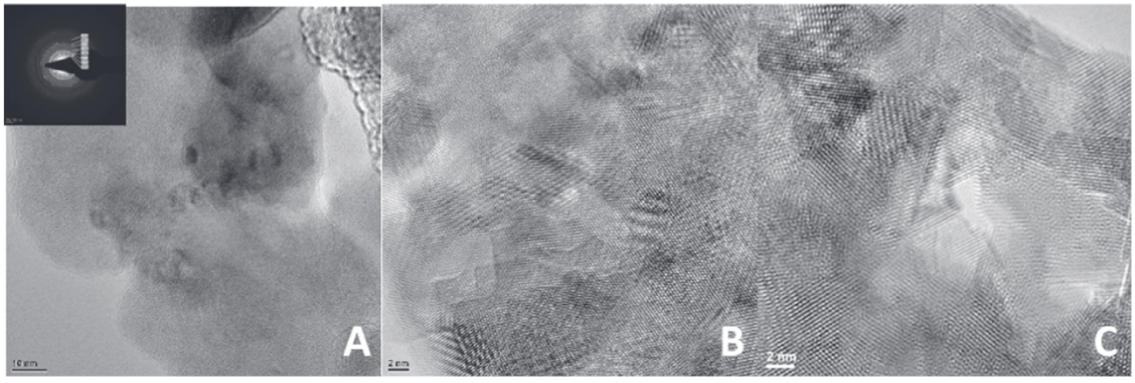

b) SiO_2-Ag-Gr: A) Light field transmission electron microscopy image showing a set of SiO_2-Ag-Gr nanoparticles, evidencing the transparent, layered, and folded structure of graphene, but decorated with SiO_2 particles, having mainly spherical shape and nanometric dimensions. The SiO_2 nanoparticles appear randomly distributed on Gr surface with a tendency to produce larger agglomerates of nanometric dimensions. High resolution electron diffraction imaging in B) and C) confirm the nature of these filler. Smaller crystalline particles associated with a high-contrast surface are observed.

Fig. 4. *Light field transmission electron microscopy (TEMBF) image and electron diffraction image (SAED) image associated with high resolution transmission electron microscopy (HRTEM) for the synthesized powders: a) HA-Ag and b) SiO_2-Ag-Gr.* a) HA-Ag: A) Light field transmission electron microscopy imaging showing a set of hydroxyapatite and silver nanoparticles in form of rods; B) and C) associated electron diffraction imaging (SAED) with high resolution transmission imaging (HRTEM) evidencing a HA nano-crystalline area at two different resolutions. The very bright spots belong to large HA crystallites and the small spots correspond to very small nanocrystals. Diameter diffraction circles correspond to interplanetary distances specific to the families of crystalline planes (indexed in the image) of the compound $Ca_5(PO_4)_3OH$ with hexagonal crystal lattice. *b) SiO_2-Ag-Gr*: A) Light field transmission electron microscopy image showing a set of SiO_2-Ag-Gr nanoparticles, evidencing the transparent, layered, and folded structure of graphene, but decorated with SiO_2 particles, having mainly spherical shape and nanometric dimensions. The SiO_2 nanoparticles appear randomly distributed on Gr surface with a tendency to produce larger agglomerates of nanometric dimensions. High resolution electron diffraction imaging in B) and C) confirm the nature of these filler. Smaller crystalline particles associated with a high-contrast surface are observed.

significantly stronger adhesion of the reference adhesive to dentin was observed, while the experimental adhesives undoubtedly adhered better to the resin composite. This is consistent with the previously exposed arguments, as the bond of 10-MDP to the HA of dentin is far stronger than the van der Waals forces and hydrogen bonds that occur between the micromechanical interlocked experimental adhesives and dentine [45]. In addition, self-assembled nano-layered structures were observed in the 10-MDP and hydroxyapatite interaction [56], which were associated with an strengthening effect manifested on the hybrid layer, the

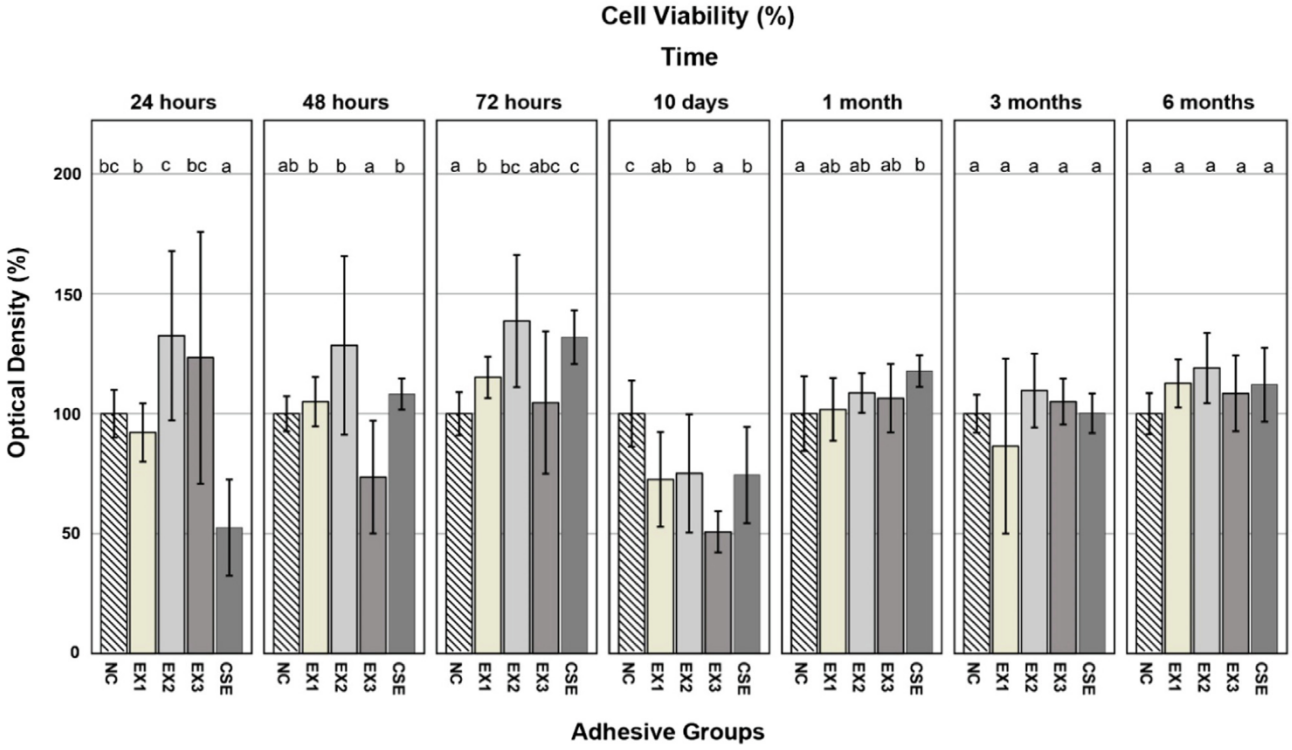

Fig. 5. Optical densities OD (mean and standard deviation) in percentage of NC = negative control, ordered by elution time. Different superscripts indicate statistically significant differences between analyzed adhesives and the NC. If two or more columns contain the same letter, no statistically significant differences were found between those groups. The same rule applies in columns with more than one letter. Tukey's HSD post-hoc test ($\alpha = 0.05$) and Games - Howell post-hoc test ($\alpha = 0.05$).

adhesive layer, but also their interaction [57]. These observation motivate the further development of the experimental adhesives described here in terms of their application method, in which a self-etching primer is to be considered instead of the phosphoric acid etching in order to take advantage of an additional long-term chemical interaction with the tooth structure. On a positive note, all fractures occurred adhesively, in other words at the interface between RBC and dentin, which allows the conclusion that the measured data relates indeed to the bond strength.

In terms of adhesive layer thickness, all adhesives performed equally. In contrast, EX2 differed significantly from the reference in terms of RTPN, evidencing the lowest infiltration. While effects such as particle agglomerations in adhesives can obturate dentinal tubules and prevent infiltration of the adhesive monomers into the demineralized dentin, there is no evidence that the thickness of the adhesive layer and the number of resin tags formed lead to better mechanical properties [58,59], which is confirmed by the present data. On the other hand some authors state that improved bond strength can be achieved through the presence of lateral branches as a result of dissolution of the peritubular dentin [60]. The presence of lateral branches could, however, not be detected in our SEM evaluation for either the experimental or the reference adhesives.

Since dental adhesives come into direct contact with biological tissue, the assessment of their cytotoxicity and biocompatibility is mandatory. The HGF-1 cell line is widely used in the biological evaluation of dental materials because gingival fibroblasts come in proximity of dental materials in clinical conditions [61]. The WST-1 assay was chosen to assess cell viability as it has a wide linear range and yields a water-soluble cleavage product whose amount directly correlates with the number of metabolic active cells in the culture. Moreover, working with an established and well characterized cell line provides a useful opportunity for a standardized and reproducible measurement of cell proliferation, independent of individual donor differences. The ISO 10993–5 defines that a medical material has cytotoxic potential if the cell viability is lower than 70 % compared to the negative control used in the experiment. Thus, the experimental adhesives in this study did not show significant cytotoxicity at any elution periods tested, except for the 10-day eluates, where the EX3 showed significantly higher toxicity compared to the negative control. Although not considered potentially cytotoxic under the mentioned ISO conditions, in the 10-day eluates we also observed a mild cytotoxic effect with evident cell growth inhibition for EX1 (73% viability vs. control) and EX2 (75%), which was comparable to the gold standard CSE (74%). The reason therefore is the fact that the 10-day eluates cumulate the elution of a larger period, from day 3 to day 10. In the following long-term tests, none of the experimental adhesives showed any cytotoxic effects, making them suitable for potential use in humans. On a general note, adhesive toxicity is mainly attributed to the presence of residual monomers that may be eluted. Even with sufficient light-curing, adhesive systems form a thin oxygen-inhibited layer on the outer surface during polymerization, leaving a thin, insufficiently cured layer [51] with potential residual monomers. These residual monomers can not only act as plasticizers and reduce mechanical properties, but also negatively affect biocompatibility [62]. Solvents such as water penetrate the polymer network, causing expansion of the polymer structure, facilitating the extraction of residual unreacted monomers and promoting the dissolution of linear polymer chains. Since HEMA is a co-monomer used in most dental adhesives, including the adhesives analyzed in the present study, its toxicological potential has been extensively analyzed. It was found in eluates from commercial adhesives together with TEGDMA, another commonly used co-monomer in adhesives, but also with unreacted photoinitiator molecules (e.g. camphorquinone) and proved to be cytotoxic on 3T3 fibroblasts [63]. In particular, HEMA has been reported to cause cell death and induce cell cycle delay in human

pulp fibroblasts and human gingival epithelial S-G cells in a concentration-dependent manner [64]. It can increase the production of reactive oxygen species (ROS) and deplete intracellular glutathione (GSH), which can lead to a delay in cell cycle progression [64,65]. Because HEMA was present in both the primer and the adhesive of the gold standard reference, but only in small amounts in the experimental adhesives, it can be held responsible for the initially higher toxicity of the former. However, since the experimental adhesives also contain TEGDMA and bis-GMA in addition to HEMA, all of which are cytotoxic and can trigger concentration-dependent cell death [66], the functionalized filler apparently compensates for this effect. It should be mentioned in this context that graphene-based materials can be both biocompatible and toxic to living cells [67] depending on layer number, lateral size, purity, dose, surface chemistry and hydrophilicity [68]. The cytotoxicity of graphene is mainly attributed to the formation of ROS in the cytosol leading to changes in cell structure and the metabolic activity [69]. In our study, the integration of functionalized graphene particles had a positive impact on toxicity, resulting in good biocompatibility of the experimental adhesives. This is in line with other studies that have shown that GO-Ag nanocomposites could exhibit negligible toxicity on HEK 293 cells [70] and that experimental graphene based dental resin composites (rGO/ZrO_2; HA-Zr; silica BaO glass nanofiller) did not exhibit cytotoxic effects on dental pulp fibroblasts when compared to untreated cells [71].

5. Conclusions

Functionalized graphene and hydroxyapatite nano-powders enabled synthesis of non-toxic dental adhesives. The improvement is particularly evident in the early elution phase (24 h) when the gold standard adhesive used as reference was cytotoxic. In the same aging period, the bond to dentin was more reliable in the experimental adhesives compared to the clinically established adhesive. Thermal aging slightly alters the long-term bonding effectiveness in two of three experimental groups, which must be related to the interaction mechanisms with the dentine. Dental adhesives with functionalized graphene and hydroxyapatite fillers can be promising candidates for future use in dental applications in clinical conditions.

6. Data availability:

The raw data required to reproduce these findings are available on request.

Funding

This research did not receive any specific grant from funding agencies in the public, commercial, or not-for-profit sectors.

Declaration of Competing Interest

The authors declare that they have no known competing financial interests or personal relationships that could have appeared to influence the work reported in this paper.

Acknowledgments:

The authors are grateful to Kuraray Co.Ltd and Voco GmbH for providing us with the comercial adhesive used as reference and the resin-based composite.

References

[1] F.N. Hugo, N.J. Kassebaum, W. Marcenes, E. Bernabé, Role of dentistry in global health: challenges and research priorities, J. Dent. Res. 100 (7) (2021) 681–685, https://doi.org/10.1177/0022034521992011.
[2] R. Montag, W. Dietz, S. Nietzsche, T. Lang, K. Weich, B.W. Sigusch, P. Gaengler, Clinical and micromorphologic 29-year results of Posterior composite restorations, J. Dent. Res. 97 (13) (2018) 1431–1437, https://doi.org/10.1177/0022034518788798.
[3] U. Pallesen, J.W. van Dijken, A randomized controlled 27 years follow up of three resin composites in class II restorations, J. Dent. 43 (12) (2015) 1547–1558, https://doi.org/10.1016/j.jdent.2015.09.003.
[4] H.V. Worthington, S. Khangura, K. Seal, M. Mierzwinski-Urban, A. Veitz-Keenan, P. Sahrmann, P.R. Schmidlin, D. Davis, Z. Iheozor-Ejiofor, M.G. Rasines Alcaraz, Direct composite resin fillings versus amalgam fillings for permanent posterior teeth, Cochrane Database Syst Rev 8(8) (2021) Cd005620.10.1002/14651858.CD005620.pub3.
[5] M.A. Coulter, Minamata Convention on Mercury, Int. Legal Mater. 55 (3) (2016) 582–616, https://doi.org/10.5305/intelegamate.55.3.0582.
[6] C.A. Stewart, Y. Finer, Biostable, antidegradative and antimicrobial restorative systems based on host-biomaterials and microbial interactions, Dent. Mater. 35 (1) (2019) 36–52, https://doi.org/10.1016/j.dental.2018.09.013.
[7] D. Dionysopoulos, O. Gerasimidou, C. Papadopoulos, Current modifications of dental adhesive systems for composite resin restorations: a review in literature, Journal of Adhesion Science and Technology 36(5) (2022) 453-468.10.1080/01694243.2021.1924499.
[8] B. Van Meerbeek, G. Willems, J.P. Celis, J.R. Roos, M. Braem, P. Lambrechts, G. Vanherle, Assessment by nano-indentation of the hardness and elasticity of the resin-dentin bonding area, J. Dent. Res. 72 (10) (1993) 1434–1442, https://doi.org/10.1177/00220345930720101401.
[9] J.P. Davim, Biomedical Composites, De Gruyter, Berlin, Boston, 2013.
[10] I. Farooq, S. Ali, S. Al-Saleh, E.M. AlHamdan, M.H. AlRefeai, T. Abduljabbar, F. Vohra, Synergistic Effect of Bioactive Inorganic Fillers in Enhancing Properties of Dentin Adhesives-A Review, Polymers 13(13) (2021).10.3390/polym13132169.
[11] K.S. Novoselov, A.K. Geim, S.V. Morozov, D. Jiang, Y. Zhang, S.V. Dubonos, I.V. Grigorieva, A.A. Firsov, Electric field effect in atomically thin carbon films, Science 306 (5696) (2004) 666–669, https://doi.org/10.1126/science.1102896.
[12] A.K. Geim, K.S. Novoselov, The rise of graphene, Nat. Mater. 6 (3) (2007) 183–191, https://doi.org/10.1038/nmat1849.
[13] A.M. Jastrzębska, P. Kurtycz, A.R. Olszyna, Recent advances in graphene family materials toxicity investigations, J. Nanoparticle Res. 14 (12) (2012) 1320, https://doi.org/10.1007/s11051-012-1320-8.
[14] A.H. Castro Neto, F. Guinea, N.M.R. Peres, K.S. Novoselov, A.K. Geim, The electronic properties of graphene, Reviews of Modern Physics 81(1) (2009) 109-162.10.1103/RevModPhys.81.109.
[15] A.A. Balandin, Thermal properties of graphene and nanostructured carbon materials, Nat. Mater. 10 (8) (2011) 569–581, https://doi.org/10.1038/nmat3064.
[16] C. Lee, X. Wei, J.W. Kysar, J. Hone, Measurement of the elastic properties and intrinsic strength of monolayer graphene, Science 321 (5887) (2008) 385–388, https://doi.org/10.1126/science.1157996.
[17] H. Xie, T. Cao, F.J. Rodríguez-Lozano, E.K. Luong-Van, V. Rosa, Graphene for the development of the next-generation of biocomposites for dental and medical applications, Dent. Mater. 33 (7) (2017) 765–774, https://doi.org/10.1016/j.dental.2017.04.008.
[18] K.S. Novoselov, V.I. Fal'ko, L. Colombo, P.R. Gellert, M.G. Schwab, K. Kim, A roadmap for graphene, Nature 490 (7419) (2012) 192–200, https://doi.org/10.1038/nature11458.
[19] K. Chen, X. Tang, B. Jia, C. Chao, Y. Wei, J. Hou, L. Dong, X. Deng, T.H. Xiao, K. Goda, L. Guo, Graphene oxide bulk material reinforced by heterophase platelets with multiscale interface crosslinking, Nat. mater. (2022), https://doi.org/10.1038/s41563-022-01292-4.
[20] N. Ilie, C. Sarosi, M.-C. Rosu, M. Moldovan, Synthesis and characterization of graphene oxide-zirconia (GO-ZrO2) and hydroxyapatite-zirconia (HA-ZrO2) nano-fillers for resin-based composites for load-bearing applications, J. Dent. 105 (2021), https://doi.org/10.1016/j.jdent.2020.103557 103557.
[21] A.C. Ionescu, E. Brambilla, P.M. Pires, A. López-Castellano, A.M. Alambiaga-Caravaca, C. Lenardi, S. Sauro, Physical-chemical and microbiological performances of graphene-doped PMMA for CAD/CAM applications before and after accelerated aging protocols, Dent. Mater. (2022), https://doi.org/10.1016/j.dental.2022.06.032.
[22] S.-M. Lee, K.-H. Yoo, S.-Y. Yoon, I.-R. Kim, B.-S. Park, W.-S. Son, C.-C. Ko, S.-A. Son, Y.-I. Kim, Enamel anti-demineralization effect of orthodontic adhesive containing bioactive glass and graphene oxide: an in-vitro study, Materials 11 (9) (2018) 1728.
[23] Y.F. AlFawaz, B. Almutairi, H.F. Kattan, M.S. Zafar, I. Farooq, M. Naseem, F. Vohra, T. Abduljabbar, Dentin Bond Integrity of Hydroxyapatite Containing Resin Adhesive Enhanced with Graphene Oxide Nano-Particles-An SEM, EDX, Micro-Raman, and Microtensile Bond Strength Study, Polymers (Basel) 12(12) (2020) 2978.10.3390/polym12122978.
[24] Z. Jia, X. Feng, Y. Zou, Graphene reinforced epoxy adhesive for fracture resistance, Composites Part B: Eng. 155 (2018) 457–462, https://doi.org/10.1016/j.compositesb.2018.09.093.
[25] R.N. Jardim, A.A. Rocha, A.M. Rossi, A. de Almeida Neves, M.B. Portela, R.T. Lopes, T.M. Pires dos Santos, Y. Xing, E. Moreira da Silva, Fabrication and

characterization of remineralizing dental composites containing hydroxyapatite nanoparticles, Journal of the Mechanical Behavior of Biomedical Materials 109 (2020) 103817.10.1016/j.jmbbm.2020.103817.
[26] V.C.B. Leitune, F.M. Collares, R.M. Trommer, D.G. Andrioli, C.P. Bergmann, S.M. W. Samuel, The addition of nanostructured hydroxyapatite to an experimental adhesive resin, J. dent. 41 (4) (2013) 321–327, https://doi.org/10.1016/j.jdent.2013.01.001.
[27] M. Sadat-Shojai, M. Atai, A. Nodehi, L.N. Khanlar, Hydroxyapatite nanorods as novel fillers for improving the properties of dental adhesives: synthesis and application, Dent. Mater. 26 (5) (2010) 471–482, https://doi.org/10.1016/j.dental.2010.01.005.
[28] L. Chen, S. Chai, K. Liu, N. Ning, J. Gao, Q. Liu, F. Chen, Q. Fu, enhanced epoxy/silica composites mechanical properties by introducing graphene oxide to the interface, ACS Appl. Mater. Interfaces 4 (8) (2012) 4398–4404, https://doi.org/10.1021/am3010576.
[29] H.W. Liu Mei, Chen Wenjing, Hu Xiaokun, Graphene Oxide-Silica Composite Fillers into the Experimental Dental Adhesives for Potential Therapy, 1(2) (2017) 42-46.10.21127/yaoyimr20170012.
[30] L. Ge, Q. Li, M. Wang, J. Ouyang, X. Li, M.M.Q. Xing, Nanosilver particles in medical applications: synthesis, performance, and toxicity, Int. J. Nanomed. 9 (2014) 2399–2407, https://doi.org/10.2147/IJN.S55015.
[31] M. Dutra-Correa, A.A.B.V. Leite, S.P.H.M. de Cara, I.M.A. Diniz, M.M. Marques, I. B. Suffredini, M.S. Fernandes, S.H. Toma, K. Araki, I.S. Medeiros, Antibacterial effects and cytotoxicity of an adhesive containing low concentration of silver nanoparticles, J. Dent. 77 (2018) 66–71, https://doi.org/10.1016/j.jdent.2018.07.010.
[32] C. Prejmerean, M. Moldovan, L. Silaghi-Dumitrescu, D. Prodan, G. Furtos, M. Trif, V. Popescu, V. Pascalau, C. Petrea, R. Silaghi-Dumitrescu, Composition Versus Physico-mechanical Properties of Some Dental Experimental Polymers, Mater. Plast. 48 (1) (2011).
[33] M.H. Santos, M.d. Oliveira, L.P.d.F. Souza, H.S. Mansur, W.L. Vasconcelos, Synthesis control and characterization of hydroxyapatite prepared by wet precipitation process %J, Mater. Res. 7 (4) (2004) 625–630.
[34] W.S. Hummers, R.E. Offeman, Preparation of Graphitic Oxide, Journal of the American Chemical Society 80(6) (1958) 1339-1339.10.1021/ja01539a017.
[35] L. Perinka, H. Sano, H. Hosoda, Dentin thickness, hardness, and Ca-concentration vs bond strength of dentin adhesives, Dent. Mater. 8 (4) (1992) 229–233, https://doi.org/10.1016/0109-5641(92)90090-Y.
[36] I. Watanabe, N. Nakabayashi, D.H. Pashley, Bonding to Ground Dentin by a Phenyl-P Self -etching Primer, J. Dent. Res. 73 (6) (1994) 1212–1220, https://doi.org/10.1177/00220345940730061301.
[37] H. Schweikl, K.-A. Hiller, C. Bolay, M. Kreissl, W. Kreismann, A. Nusser, S. Steinhauser, J. Wieczorek, R. Vasold, G. Schmalz, Cytotoxic and mutagenic effects of dental composite materials, Biomaterials 26 (14) (2005) 1713–1719, https://doi.org/10.1016/j.biomaterials.2004.05.025.
[38] Sigma - Aldrich, Protocol Guide: WST-1 Assay for Cell Proliferation and Viability. https://www.sigmaaldrich.com/technical-documents/protocols/biology/roche/cell-proliferation-reagent-wst-1.html.
[39] ISO10993-5:2009, Biological evaluation of medical devices — Part 5: Tests for in vitro cytotoxicity, 2017.
[40] S. Liu, T.H. Zeng, M. Hofmann, E. Burcombe, J. Wei, R. Jiang, J. Kong, Y. Chen, Antibacterial activity of graphite, graphite oxide, graphene oxide, and reduced graphene oxide: membrane and oxidative stress, ACS Nano. 5 (9) (2011) 6971–6980, https://doi.org/10.1021/nn202451x.
[41] O. Akhavan, E. Ghaderi, A. Esfandiar, Wrapping bacteria by graphene nanosheets for isolation from environment, reactivation by sonication, and inactivation by near-infrared irradiation, j. phys. Chem. B 115 (19) (2011) 6279–6288, https://doi.org/10.1021/jp200686k.
[42] K. Ioannidis, S. Niazi, P. Mylonas, F. Mannocci, S. Deb, The synthesis of nano silver-graphene oxide system and its efficacy against endodontic biofilms using a novel tooth model, Dent. Mater. 35 (11) (2019) 1614–1629, https://doi.org/10.1016/j.dental.2019.08.105.
[43] A.C. Profeta, Dentine bonding agents comprising calcium-silicates to support proactive dental care: Origins, development and future, Dent. Mater. J. 33 (4) (2014) 443–452, https://doi.org/10.4012/dmj.2013-267.
[44] A. Alshahrani, M.S. Bin-Shuwaish, R.S. Al-Hamdan, T. Almohareb, A.M. Maawadh, M. Al Deeb, A.M. Alhenaki, T. Abduljabbar, F. Vohra, Graphene oxide nano-filler based experimental dentine adhesive. A SEM / EDX, Micro-Raman and microtensile bond strength analysis, J Appl Biomater Funct Mater 18 (2020) 2280800020966936.10.1177/2280800020966936.
[45] M.S. Bin-Shuwaish, A.M. Maawadh, R.S. Al-Hamdan, S. Alresayes, T. Ali, B. Almutairi, F. Vohra, T. Abduljabbar, Influence of graphene oxide filler content on the dentin bond integrity, degree of conversion and bond strength of experimental adhesive. A SEM, micro-Raman, FTIR and microtensile study, Mater. Res. Express 7 (11) (2020) 115403, https://doi.org/10.1088/2053-1591/abcba7.
[46] K.S. Hui, K.N. Hui, D.A. Dinh, C.H. Tsang, Y.R. Cho, W. Zhou, X. Hong, H.-H. Chun, Green synthesis of dimension-controlled silver nanoparticle–graphene oxide with in situ ultrasonication, Acta. Materialia. 64 (2014) 326–332, https://doi.org/10.1016/j.actamat.2013.10.045.
[47] T.F. Watson, A.R. Atmeh, S. Sajini, R.J. Cook, F. Festy, Present and future of glass-ionomers and calcium-silicate cements as bioactive materials in dentistry: biophotonics-based interfacial analyses in health and disease, Dent. Mater. 30 (1) (2014) 50–61, https://doi.org/10.1016/j.dental.2013.08.202.
[48] B. Van Meerbeek, K. Yoshihara, Y. Yoshida, A. Mine, D.M. J, V.L. K.L, State of the art of self-etch adhesives, Dental Materials 27(1) (2011) 17-28.10.1016/j.dental.2010.10.023.
[49] N. Hiraishi, N. Tochio, T. Kigawa, M. Otsuki, J. Tagami, Monomer-collagen interactions studied by saturation transfer difference NMR, J. Dent. Res. 92 (3) (2013) 284–288, https://doi.org/10.1177/0022034512474310.
[50] D.H. Pashley, F.R. Tay, C. Yiu, M. Hashimoto, L. Breschi, R.M. Carvalho, S. Ito, Collagen degradation by host-derived enzymes during aging, J. Dent. Res. 83 (3) (2004) 216–221, https://doi.org/10.1177/154405910408300306.
[51] A. Apicella, L. Nicolais, Effect of water on the properties of epoxy matrix and composite, Springer, Berlin Heidelberg, Berlin, Heidelberg, 1985, pp. 69–77.
[52] K. Cai, Y. Delaviz, M. Banh, Y. Guo, J.P. Santerre, Biodegradation of composite resin with ester linkages: identifying human salivary enzyme activity with a potential role in the esterolytic process, Dent. Mater. 30 (8) (2014) 848–860, https://doi.org/10.1016/j.dental.2014.05.031.
[53] I.M. Barszczewska-Rybarek, A Guide through the Dental Dimethacrylate Polymer Network Structural Characterization and Interpretation of Physico-Mechanical Properties, Materials (Basel) 12(24) (2019).10.3390/ma12244057.
[54] M. Freund, E.C. Munksgaard, Enzymatic degradation of BISGMA/TEGDMA-polymers causing decreased microhardness and greater wear in vitro, Scandinavian j. dent. Res. 98 (4) (1990) 351–355, https://doi.org/10.1111/j.1600-0722.1990.tb00984.x.
[55] Y. Nishitani, M. Yoshiyama, K. Hosaka, J. Tagami, A. Donnelly, M. Carrilho, F.R. Tay, D.H. Pashley, Use of Hoy's solubility parameters to predict water sorption/solubility of experimental primers and adhesives 115 (1) (2007) 81–86, https://doi.org/10.1111/j.1600-0722.2007.00430.x.
[56] K. Yoshihara, Y. Yoshida, N. Nagaoka, D. Fukegawa, S. Hayakawa, A. Mine, M. Nakamura, S. Minagi, A. Osaka, K. Suzuki, B. Van Meerbeek, Nano-controlled molecular interaction at adhesive interfaces for hard tissue reconstruction, Acta. Biomaterialia. 6 (9) (2010) 3573–3582, https://doi.org/10.1016/j.actbio.2010.03.024.
[57] K. Yoshihara, N. Nagaoka, A. Nakamura, T. Hara, Y. Yoshida, B. Van Meerbeek, Nano-layering adds strength to the adhesive interface, J. Dent. Res. 100 (5) (2021) 515–521, https://doi.org/10.1177/0022034520979133.
[58] E. Lodovici, A. Reis, S. Geraldeli, J.L. Ferracane, R.Y. Ballester, L.E.R. Filho, Does adhesive thickness affect resin-dentin bond strength after thermal/load cycling?, Operative Dent 34 (1) (2009) 58–64, https://doi.org/10.2341/08-37.
[59] U. Lohbauer, S.A. Nikolaenko, A. Petschelt, R. Frankenberger, Resin tags do not contribute to dentin adhesion in self-etching adhesives, J. Adhes. Dent. 10 (2) (2008) 97–103.
[60] M. Ferrari, C.L. Davidson, In vivo resin-dentin interdiffusion and tag formation with lateral branches of two adhesive systems, J. Prosthetic Dent. 76 (3) (1996) 250–253, https://doi.org/10.1016/S0022-3913(96)90167-5.
[61] G.L. Polyzois, In vitro evaluation of dental materials, Clin. Mater. 16 (1) (1994) 21–60, https://doi.org/10.1016/0267-6605(94)90088-4.
[62] I.E. Ruyter, Unpolymerized surface layers on sealants, Acta. Odontologica. Scandinavica. 39 (1) (1981) 27–32, https://doi.org/10.3109/00016358109162255.
[63] W. Geurtsen, W. Spahl, K. Muller, G. Leyhausen, Aqueous extracts from dentin adhesives contain cytotoxic chemicals, J. Biomed. Mater. Res. 48 (6) (1999) 772–777.
[64] H.-H. Chang, M.-K. Guo, F.H. Kasten, M.-C. Chang, G.-F. Huang, Y.-L. Wang, R.-S. Wang, J.-H. Jeng, Stimulation of glutathione depletion, ROS production and cell cycle arrest of dental pulp cells and gingival epithelial cells by HEMA, Biomaterials 26 (7) (2005) 745–753, https://doi.org/10.1016/j.biomaterials.2004.03.021.
[65] G. Spagnuolo, C. Mauro, A. Leonardi, M. Santillo, R. Paternò, H. Schweikl, E.V. Avvedimento, S. Rengo, NF-κB Protection against Apoptosis Induced by HEMA, J. Dental Res. 83 (11) (2004) 837–842, https://doi.org/10.1177/154405910408301103.
[66] M. Kusdemir, S. Gunal, F. Ozer, S. Imazato, N. Izutani, S. Ebisu, M.B. Blatz, Evaluation of cytotoxic effects of six self-etching adhesives with direct and indirect contact tests, Dent Mater. J. 30 (6) (2011) 799–805, https://doi.org/10.4012/dmj.2011-046.
[67] M. Tahriri, M. Del Monico, A. Moghanian, M. Tavakkoli Yaraki, R. Torres, A. Yadegari, L. Tayebi, Graphene and its derivatives: Opportunities and challenges in dentistry, Materials Science and Engineering: C 102 (2019) 171-185.10.1016/j.msec.2019.04.051.
[68] C. Liao, Y. Li, S.C. Tjong, Graphene Nanomaterials: Synthesis, Biocompatibility, and Cytotoxicity, Int J Mol Sci 19(11) (2018) 3564.10.3390/ijms19113564.
[69] K.-H. Liao, Y.-S. Lin, C.W. Macosko, C.L. Haynes, Cytotoxicity of graphene oxide and graphene in human erythrocytes and skin fibroblasts, ACS Appl. Mater. Interfaces 3 (7) (2011) 2607–2615, https://doi.org/10.1021/am200428v.
[70] W. Shao, X. Liu, H. Min, G. Dong, Q. Feng, S. Zuo, Preparation, characterization, and antibacterial activity of silver nanoparticle-decorated graphene oxide nanocomposite, ACS Appl. Mater. Interfaces 7 (12) (2015) 6966–6973, https://doi.org/10.1021/acsami.5b00937.
[71] A. Dreanca, C. Sarosi, A.E. Parvu, M. Blidaru, G. Enacrachi, R. Purdoiu, A. Nagy, B. Sevastre, N.A. Oros, I. Marcus, M. Moldovan, Systemic and local biocompatibility assessment of graphene composite dental materials in experimental mandibular bone defect, Materials 13 (11) (2020) 2511.